

QUARK-GLUON PLASMAS AND THERMALIZATION *

PETER ARNOLD

*Department of Physics, University of Virginia, P.O. Box 400714
Charlottesville, VA 22904-4714, U.S.A.*

parnold@virginia.edu

In these lectures, I will attempt a pedagogical and qualitative introduction to the theory of equilibrium and thermalization of quark-gluon plasmas. I assume only that the reader is familiar with quantum field theory at zero temperature and with QCD as the theory of the strong interactions. I focus on the limit of small α_s , which in principle should be relevant at extremely high temperature because of asymptotic freedom, and in any case provides a clean theoretical context in which to discuss a variety of phenomena. Topics discussed include the basic equilibrium formalism for finite-temperature quantum field theory, Debye screening, electric deconfinement, magnetic confinement, dimensional reduction, plasma waves, kinetic theory, hydrodynamic properties such as viscosity, the Landau-Pomeranchuk-Migdal effect, thermalization in (arbitrarily high energy) heavy ion collisions, and QCD plasma instabilities.

1. Introduction to Quark-Gluon Plasma

Imagine a perfect container filled with nothing but vacuum. What happens if we slowly heat it? At first, blackbody photons appear inside the container. As we increase the temperature, the density (and energy) of blackbody photons increases. Once we raise the temperature to the neighborhood of $m_e c^2 \simeq 0.5$ MeV, something interesting happens. The photons have enough energy to pair produce and make pairs of electrons and positrons.

Now consider even higher temperature of order $k_B T \sim 50$ MeV. A few photons will have enough energy to pair produce pions ($m_\pi c^2 \simeq 135$ MeV), yielding a dilute gas of pions inside the container (in addition to the photons and electrons). Each individual pion, of course, is a finite-size object made up of a quark and anti-quark in the non-relativistic quark model (and containing other quark/anti-quark pairs and gluons if we look close enough to resolve the structure on smaller distance scales), held together by confinement. As we continue to increase the temperature, the density of pions increases and increases, until eventually the pions are so dense that they overlap at temperatures of order the QCD scale, $k_B T \sim 200$ MeV. And if the pions overlap, how is a quark to know which other partons it is bound to by confinement? This is a standard cartoon picture of deconfinement at high temperature. At high enough temperature, the quarks and gluons become so dense that

*Based on lectures given at X Hadron Physics in Florianópolis, SC, Brazil, March 26–31, 2007.

they lose track of who they are confined with and so can individually wander across the system. The important point here is that, for ultra-relativistic temperatures, higher temperature means higher *density* as well as higher energy.

As we increase the temperature further to $k_B T \gg 200$ MeV, the density of quarks and gluons increases, just as the density of photons did. And since their energies are of order T , one expects that the running coupling α_s should be $\alpha_s(T)$. By asymptotic freedom, this gas of quarks and gluons will become weakly coupled if we go to very large T .

Historically, the temperatures necessary for a quark-gluon plasma (QGP) existed up until the Universe was about a millionth of a second old. Experimentally, quark gluon plasmas are believed to be created in sufficiently energetic heavy ion collisions, such as the RHIC experiment at Brookhaven National Lab, where, for example, gold nuclei are collided at energies of order 100 GeV per nucleon.

In the context of heavy ion collisions, this lecture will nicely complement the lecture by Francois Gelis¹ in this series. In a heavy ion collision at very high energies, the theoretical picture is that the colliding ions create a “color glass condensate,” which eventually thermalizes to make a quark-gluon plasma in local thermal equilibrium. Francois’s lectures take us forward in time up through the creation of the color glass condensate. I will instead work backwards in time, starting from a description of equilibrium. Then I discuss the relaxation of small departures from equilibrium (relevant to slightly earlier times). I conclude with the physics of equilibration from very non-equilibrium initial conditions such as the color glass condensate.

1.1. *Introduction to weak coupling*

A theorist’s first instinct when confronted with any field theory problem is generally to wonder if it can be solved for weak coupling. In this case, that means $\alpha_s(T) \ll 1$.

Let me first give you some examples of static equilibrium quantities. The free energy has the weak coupling expansion²

$$F = \#T^4[1 + \#g^2 + \#g^3 + g^4(\# \ln g + \#) + \#g^5 + g^6(\# \ln g + \#) + \dots], \quad (1)$$

where all the numerical coefficients $\#$ are known except for the last (boldface) one. It may seem a little strange that the expansion has odd powers of g and factors of $\ln g$, since perturbation theory is generally an expansion in g^2 . What’s stranger is that the last, unknown numerical coefficient (the coefficient of g^6) is not a perturbative quantity at all: its value depends on fundamentally non-perturbative physics (as do yet other coefficients at yet higher orders). We’ll discuss how this can be in a moment, but it exemplifies an important point for studying thermal gauge theories at weak coupling: the weak coupling expansion of a physical quantity is not necessarily the same thing as the *perturbative* or loop expansion of that quantity that one learns in field theory courses.

An example where non-perturbative physics crops up sooner in the expansion

is the inverse Debye screening length,³

$$\xi_D^{-1} \simeq \#gT[1 + g(\#\ln g + \#)], \quad (2)$$

where the last numerical coefficient turns out to be non-perturbative. I will discuss leading-order Debye screening a little later.

Here is an example from real-time near-equilibrium physics. The result for the shear viscosity of a QGP to leading order in powers of the coupling is known⁴ and is of the form

$$\eta = \frac{\#T^3}{g^4 \ln g} \times f\left(\frac{1}{\ln g}\right). \quad (3)$$

We'll see that this is immensely complicated in terms of diagrammatic perturbation theory. Another example (which I won't pursue in these lectures) comes from electroweak, rather than QCD plasmas, where the rate of baryon number violation in the very early universe is known to have the form⁵

$$\Gamma_B \simeq \#g^{10}T^4 \ln g, \quad (4)$$

where the numerical coefficient is non-perturbative.

Now turn to real-time, far-from-equilibrium physics. One question to ask is how long it takes for the system to equilibrate. Let's use dimensional analysis to write the leading-order answer to this question in the form

$$t_{\text{eq}} \sim \frac{g^{-??}}{\text{momentum scale}}, \quad (5)$$

where "momentum scale" is the relevant momentum scale of the problem. The situation here is so bad, that not even the *power* of g is known in the weak coupling limit!

1.1.1. *Small coupling \neq perturbative*

So why is the small coupling expansion not the same as the perturbative expansion at finite temperature? There's a really simple example from ordinary quantum mechanics that helps make it clear. Imagine a particle moving in a slightly anharmonic potential

$$V(x) \sim \omega_0^2 x^2 + g^2 x^4, \quad (6)$$

where g is very, very small. If we ask questions about the ground state, say, then we can approximate the potential by a harmonic oscillator and treat the quartic piece as a perturbation. The ground state wave function will extend over a range of x 's where $g^2 x^4$ is small compared to $\omega_0^2 x^2$. But now imagine studying the system at high temperature, weighting the states by $\exp(-\beta E)$. As the temperature is increased, the typical energy E will increase. But high energy states probe a large range of x . (See Fig. 1.) The higher the energy, the larger the typical values of x . No matter how small g is, $g^2 x^4$ will always be bigger than $\omega_0^2 x^2$ for large enough x . So, at high enough temperature, a perturbative treatment of $g^2 x^4$ breaks down.

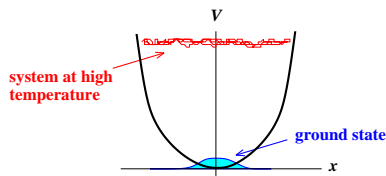


Fig. 1. A slightly anharmonic potential.

Note that in this example the break down of perturbation theory corresponds to high energies, which is also the limit where the physics of the problem is *classical*. We will be led to deal with analogous non-perturbative problems in weakly-coupled quantum field theory by recasting them as problems in *classical* field theory.

In my example, I phrased the problem as one of high temperatures T for fixed potential $V(x)$. However, I would have encountered the same problem if I had held T and g fixed but decreased ω_0 : eventually, $g^4 x^4$ would win over $\omega_0^2 x^2$. In gauge theory, the frequency ω_k of a field mode with wavenumber k is $\omega_k \sim k$. So, at fixed temperature, I may expect a problem with perturbation theory as I consider the physics $\omega_k \sim k \rightarrow 0$ of sufficiently long wavelength modes. We will see that this is the case.

1.1.2. Are RHIC QGPs weakly coupled?

Theorists try to obtain insight by solving the problems that they can, which are not always the problems directly relevant to experiment. At RHIC, it is estimated that the quark-gluon plasma may have a temperature of order $T \sim 2T_c \sim 350$ MeV, where T_c is the transition temperature from a hadron gas to a quark-gluon plasma. So, is $\alpha_s(350 \text{ MeV})$ a small number? This seems ridiculous.

Historically, however, certain lattice QCD results lent people optimism that weak coupling might not be such a terrible approximation after all. To understand this, let's focus on the energy density of an ideal gas, where particles are not coupled at all. First, let me remind you of the standard Stefan-Boltzmann result for the energy density ϵ of an ideal gas of photons, which is

$$\epsilon = 2 \times \frac{\pi^2}{30} T^4. \quad (7)$$

Here and throughout, I work in units where $\hbar = c = k_B = 1$. The T^4 comes from simple dimensional analysis. The factor of 2 out front represents the two possible polarizations of a photon in a mode with a given wavenumber \mathbf{k} , and the $\pi^2/30$ is a numerical factor that you learned to compute in a Statistical Mechanics course. For an ideal gas of massless pions (i.e. at temperatures large compared to the pion mass), the result would be

$$\epsilon = 3 \times \frac{\pi^2}{30} T^4. \quad (8)$$

Pions have no spin (and so no polarization) and the 3 counts the different types π^0 , π^+ , and π^- of pions. Similarly, for a quark-gluon plasma with massless u , d , and s quarks, one gets

$$\epsilon = 47.5 \times \frac{\pi^2}{30} T^4. \quad (9)$$

Here, the large factor in front counts (i) three flavors of quarks with three colors and two spin states, (ii) the anti-quarks, and (iii) eight colors of gluons with two polarizations. (It's not an integer because the fermions get a slightly different factor than $\pi^2/30$ because of the difference between Fermi and Bose statistics.) Now look, for example, at the lattice data of Karsch *et al.*⁶ shown in Fig. 2. It shows ϵ/T^4 plotted vs. T . At high temperature, the curve to look at is the upper one, corresponding to three massless flavors. The arrow labeled ϵ_{SB}/T^4 in the upper-right corner shows the 3-flavor Stefan-Boltzmann result (9). As you can see, it is off by a little over 20%. So, from this measurement alone, treating the system as a nearly ideal gas of quarks and gluons does not look too bad. The sudden jump in ϵ/T^4 from low temperature to high temperature can crudely be interpreted as a sudden jump in the number of degrees of freedom going from a pion gas (8) to a quark-gluon plasma (9).

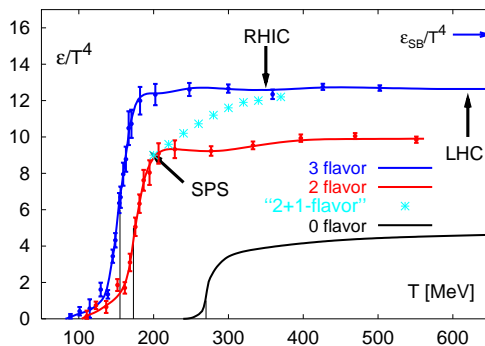


Fig. 2. Lattice data on energy density in units of T^4 from Karsch *et al.*⁶

The problem, however, is that approximate ideal gas behavior is not a sure sign of weak coupling. There is an important theoretical counter-example. Instead of QCD, consider the related theory of supersymmetric $SU(N_c)$ Yang-Mills theory with four super-symmetries ($\mathcal{N} = 4$). This is a conformal theory with vanishing β function. Then take the large N_c limit ($N_c \rightarrow \infty$ with $g^2 N_c$ fixed). Finally, take the infinite 't Hooft coupling limit $g^2 N_c \rightarrow \infty$. This strongly-coupled four-dimensional theory has been solved using the AdS/CFT conjecture to map it into a problem of classical gravity of a black brane in five-dimensional anti-deSitter space.⁷ The

result is

$$\epsilon = 0.75 \epsilon_{\text{ideal}}, \quad (10)$$

which is roughly the difference we saw in Fig. 2. Indeed, some people, pointing to other evidence, refer to RHIC QGP's as strongly-coupled quark-gluon plasmas.⁸

The moral is that one should take weak coupling with a grain of salt for experimentally-achievable quark-gluon plasmas. However, weak coupling is a theoretically clean limit where one can make progress from first principles, and one learns a lot about the physics of finite temperature by studying it.^a

2. Static Physics in Equilibrium

2.1. *Basic equilibrium formalism*

In statistical mechanics, the basic object is the partition function Z , which can be written as

$$Z = \sum_{\text{states}} e^{-\beta E} = \sum_{\text{states}} \langle E | e^{-\beta H} | E \rangle = \text{tr} e^{-\beta H}. \quad (11)$$

Now note that $e^{-\beta H}$ can be written as a time evolution operator e^{-iHt} with imaginary time $t = -i\beta$. We know how to represent time evolution using path integrals, and so we can represent the partition function by an imaginary-time path integral:

$$Z = \int [\mathcal{D}\Phi] e^{-S_E}, \quad (12)$$

with, for example,

$$S_E = \int_0^\beta d\tau \int d^3x [(\partial\Phi)^2 + m^2\Phi^2 + \lambda\Phi^4] \quad (13)$$

and with *periodic* boundary conditions

$$\Phi(0, x) = \Phi(\beta, x) \quad (14)$$

in imaginary time for bosonic fields. These periodic boundary conditions implement the trace in $Z = \text{tr} e^{-\beta H}$. For fermionic fields, it turns out that (to implement Pauli statistics) one must impose anti-periodic boundary conditions.^b

Feynman rules are exactly the same as in zero-temperature field theory except that the imaginary time τ is now periodic with period β . To go from τ to frequency space, this means we should do a Fourier series rather than a Fourier transform. The only difference with zero-temperature Feynman rules will then be that loop frequency integrals are replaced by loop frequency sums:

$$\int \frac{d^4P}{(2\pi)^4} \rightarrow T \sum_\nu \int \frac{d^3p}{(2\pi)^3} \quad (15)$$

^aFor attempts to apply weak coupling results to experimentally relevant temperatures, see Ref. 9.

^bFor textbook treatments in the context of relativistic field theory, see Ref. 10.

with the sum over discrete imaginary-time frequencies (known as Matsubara frequencies)

$$\nu_n = 2\pi n/\beta = 2\pi nT \quad (\text{bosons}) \quad (16)$$

$$\nu_n = 2\pi(n + \frac{1}{2})/\beta = 2\pi(n + \frac{1}{2})T \quad (\text{fermions}) \quad (17)$$

to implement the periodic or anti-periodic boundary conditions.

2.1.1. An example

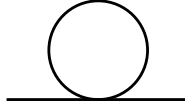


Fig. 3. A 1-loop contribution to the effective mass.

As an example, consider the self-energy diagram of Fig. 3, which contributes to the effective mass of a particle. This loop gives

$$\Delta m_{\text{eff}}^2 = \frac{\lambda}{2} T \sum_{\nu} \int \frac{d^3 p}{(2\pi)^3} \frac{1}{\nu^2 + p^2 + m^2}. \quad (18)$$

We can evaluate the sum by noticing that the Bose distribution function

$$n_{\text{B}}(\omega) = \frac{1}{e^{\beta\omega} - 1} \quad (19)$$

has simple poles with residue T at $\omega = i2\pi nT = i\nu_n$. So use the Residue Theorem to rewrite the sum (18) as

$$\Delta m_{\text{eff}}^2 = \frac{\lambda}{2} \int_C \frac{d\omega}{2\pi i} \int \frac{d^3 p}{(2\pi)^3} \frac{n_{\text{B}}(\omega)}{-\omega^2 + \omega_p^2}, \quad (20)$$

where the contour C is shown in Fig. 4a and $\omega_p^2 \equiv p^2 + m^2$. Now close each line of the contour at infinity to enclose the poles of the integrand at $\omega = \pm\omega_p$ as in Fig. 4b. Again using the Residue Theorem,^c

$$\Delta m_{\text{eff}}^2 = \int \frac{d^3 p}{(2\pi)^3 2\omega_p} \lambda n_{\text{B}}(\omega_p) + (\text{a } T=0 \text{ contribution}). \quad (21)$$

There is a simple physical way to understand the result in terms of the propagation of a particle through the thermal medium. Eq. (21) can be rewritten in the form

$$k \text{---} \text{---} \text{---} k = k \text{---} \text{---} \text{---} k \text{---} \text{---} \text{---} k - \int \frac{d^3 p}{(2\pi)^3 2\omega_p} n_{\text{B}}(\omega_p) k \text{---} \text{---} \text{---} k. \quad (22)$$

^cIt should be easy to see how the $\omega = +\omega_p$ residue works out. The $\omega = -\omega_p$ residue generates a similar result using the identity $n_{\text{B}}(-\omega_p) = -[1 + n_{\text{B}}(\omega_p)]$.

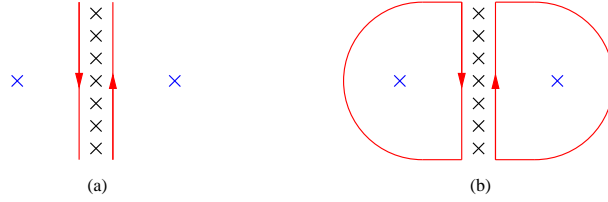


Fig. 4. Integration contour for doing frequency sum..

The last term is the amplitude for forward scattering of the particle of interest (of momentum k) off of a particle in the plasma (of momentum p), integrated over relativistic phase space, weighted by the probability density $n_B(\omega_p)$ for encountering such a particle in the plasma. In this case, the amplitude is just a factor of λ .

The moral is that the thermal contribution to the effective mass comes from forward scattering off of the medium. This is similar to the index of refraction for light in a medium, which is also caused by forward scattering and which slows light below c , like a mass does.

For future reference, note that at high temperatures ($T \gg m$), the integral in (21) is dominated by $p \sim T$, which is the momentum of typical particles in the thermal gas.

2.2. How big are loops?

Because the integral in (21) is dominated by momenta $p \sim T$, the result, by dimensional analysis, is

$$\Delta m_{\text{eff}}^2 = \# \lambda T^2 \quad (23)$$

in the high-temperature limit. The numerical coefficient is something you can easily compute by doing the integral.

For high temperatures, this loop correction to the effective mass can have a profound effect. Consider the example of high-temperature symmetry restoration. Suppose we start with a potential

$$V(\phi) = -\mu^2 \phi^2 + \lambda \phi^4 \quad (24)$$

at zero temperature. The minima of this potential are at non-zero ϕ , resulting in spontaneous symmetry breaking. However, the thermal correction to the mass will replace the $-\mu^2$ by an effective $-\mu^2 + \# \lambda T^2$:

$$V(\phi) \rightarrow (-\mu^2 + \# \lambda T^2) \phi^2 + \lambda \phi^4. \quad (25)$$

For

$$T > T_c = \frac{\mu}{(\#\lambda)^{1/2}}, \quad (26)$$

the coefficient of ϕ^2 is now positive, the minimum is at $\phi = 0$, and so thermal effects have restored the symmetry at high temperature.

The moral is that, at large enough temperature, loop effects can be large!

If loop effects are large, how can we use perturbation theory? The one-loop diagram just analyzed turns out to be the worst offender.^d So let's resum it into propagators, replacing our perturbative propagator $(P^2+m_0^2)^{-1}$ with $(P^2+m_{\text{eff}}^2)^{-1}$, where

$$m_{\text{eff}}^2 = m_0^2 + \#\lambda T^2. \quad (27)$$

That takes care of the loops like Fig. 3, but then what does it cost to add other sorts of loops to a diagram as in Fig. 5, when T is large? The cost is an explicit factor of coupling, a new loop integration, and two new propagators:

$$\lambda \times T \sum_{\nu} \int d^3p \times (\text{two propagators}). \quad (28a)$$

There's an explicit factor of λT above, and then the rest has dimensions on inverse momentum:

$$\text{cost} \sim \frac{\lambda T}{\text{momentum}}. \quad (28b)$$

The biggest cost would therefore seem to be due to the most infrared momentum. In the case at hand, the infrared is cut off by the effective mass m_{eff} , so^e

$$\text{cost} \sim \frac{\lambda T}{m_{\text{eff}}} \sim \frac{\lambda T}{(\lambda T^2)^{1/2}} \sim \sqrt{\lambda}. \quad (29)$$

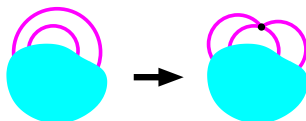


Fig. 5. Generically adding another loop to a diagram.

So, for scalar theory, the small coupling expansion at high T is an expansion in $\sqrt{\lambda}$. As an example, the free energy is known to high order and has the form¹²

$$P = T^4 [1 + \#\lambda + \#\lambda^{3/2} + \#\lambda^2 + \lambda^{5/2}(\#\ln \lambda + \#) + \lambda^3(\#\ln \lambda + \#) + \dots]. \quad (30)$$

The $\ln \lambda$ comes from a logarithm $\ln(T/m_{\text{eff}})$ that arises in certain diagrams.

For scalar theory, it is enough to resum the effects of Fig. 3 into propagators to make a workable perturbation theory and, in principal, find the expansion to as high an order as one has the will to go. We'll see later that gauge theory is different.

^dFor a discussion of the size of loop effects, see the original papers on the subject.¹¹

^eThe logic here assumes that the added three-dimensional loop integral is dominated by the infrared. That's generically true, but not for insertions of Fig. 3, which gives a divergent sub-diagram that leads to an extra factor of T in its thermal contribution. But we've resummed all of those diagrams. There are also logarithmically-divergent sub-diagrams, which can give additional factors of $\ln(T/m)$.

2.3. Another way to understand $\lambda T/m$

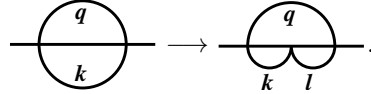
Here's another, more physical way to understand why the cost of interactions is $\lambda T/m_{\text{eff}}$ and not simply λ . Consider the limit of the Bose distribution function for small particle energies $E \ll T$:

$$n_{\text{B}}(E) = \frac{1}{e^{\beta E} - 1} \rightarrow \frac{1}{\beta E} = \frac{T}{E}. \quad (31)$$

This is largest when $E \sim m_{\text{eff}}$, giving

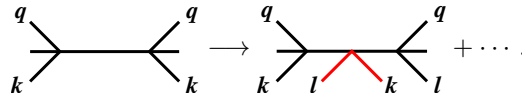
$$n_{\text{B}} \sim \frac{T}{m_{\text{eff}}}. \quad (32)$$

Now think about adding a loop, such as



$\text{---} \bigcirc \text{---} \rightarrow \text{---} \bigcirc \text{---} . \quad (33)$

In terms of forward scattering off of the medium, adding an extra interaction corresponds, for instance, to



$\begin{array}{c} q \\ \diagup \\ \text{---} \\ \diagdown \\ k \end{array} \begin{array}{c} q \\ \diagdown \\ \text{---} \\ \diagup \\ k \end{array} \rightarrow \begin{array}{c} q \\ \diagup \\ \text{---} \\ \diagdown \\ k \end{array} \begin{array}{c} q \\ \diagdown \\ \text{---} \\ \diagup \\ k \end{array} + \dots \quad (34)$

What is the cost? There is an explicit λ for the extra interaction, but there is also a factor of density $n_{\text{B}} \sim T/m_{\text{eff}}$ for the probability of an additional particle from the medium being involved. So the total cost is

$$\lambda n_{\text{B}} \sim \frac{\lambda T}{m_{\text{eff}}} \sim \sqrt{\lambda}. \quad (35)$$

In this language, we see that the T/m_{eff} factor is an enhancement due to the large density (32) of low-momentum particles in a Bose gas. (There is no similar enhancement for fermions.)

2.4. Gauge bosons “masses”

Now I'll turn to gauge theory. Suppose one evaluates one-loop self-energies like Fig. 6, plus similar diagrams with gauge boson loops. Let me consider the propagation of relatively soft gauge bosons, with ω and k small compared to T . It turns out the self-energy then has the functional form^{10,13}

$$\Pi_{\mu\nu}(\omega, k) = g^2 T^2 f_{\mu\nu}(\omega/k). \quad (36)$$

Overall, its size is determined by $g^2 T^2$, analogous to the λT^2 we discussed in the scalar case. Unlike the scalar theory, the diagram of Fig. 6 is sensitive to the external momentum, and the result turns out to depend on the ratio ω/k (and the direction of \mathbf{k}). I'm not going to give details. Instead, I will just tell you some interesting limiting cases and explain how the results make physical sense.

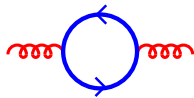


Fig. 6. A contribution to the 1-loop self-energy for gluons.

2.4.1. Debye screening

Let's consider the case $\omega = 0$ (static response). It turns out that

$$\Pi_{\nu}^{\mu} = m_{\text{D}}^2 \begin{pmatrix} 1 & & & \\ & 0 & & \\ & & 0 & \\ & & & 0 \end{pmatrix}, \quad (37)$$

where

$$m_{\text{D}}^2 = (1 + \frac{1}{6}N_{\text{f}})g^2T^2 \quad (38)$$

and N_{f} is the number of quark flavors. If we sum up insertions of this self-energy into the gauge propagator, the propagator for the electric potential A^0 at $\omega = 0$ is $(p^2 + m_{\text{D}}^2)^{-1}$. If we 3-dimensionally Fourier transform this static propagator, it should be proportional to the electric potential between two static test charges. Because of the effective mass m_{D} , this Fourier transform gives a Yukawa potential $e^{-m_{\text{D}}r}/r$ instead of the usual Coulomb $1/r$. This effect is well known in plasmas and is called Debye screening. It's something you can find discussed in detail in classical terms in Jackson.¹⁴ In our case, the corresponding screening length ξ_{D} is

$$\xi_{\text{D}} = \frac{1}{m_{\text{D}}} \sim \frac{1}{gT}. \quad (39)$$

Another way to understand color deconfinement at high temperature (i.e. the quark-gluon plasma as a nearly free gas of quarks and gluons) is in terms of Debye screening. Start by placing a negative static test charge in a QED plasma. Debye screening is caused by positive charges flying by and being bent slightly towards the test charge, while negative charges are repelled slightly away from it, so that on average there is a cloud of positive screening charge around the negative test charge. The radius of this cloud is the Debye screening length ξ_{D} , which, in both relativistic and non-relativistic situations, is order

$$\xi_{\text{D}} \sim \sqrt{\frac{T}{g^2n}}, \quad (40)$$

where n is the density of charged particles in the plasma. Outside of this radius, the average electric field falls exponentially with distance from the test charge. There is a critically important difference to notice between ultra-relativistic and non-relativistic plasmas. In the non-relativistic case, the density n is fixed, and so the Debye screening length (40) *increases* with temperature. (It's harder to bend

particles that are more energetic.) In the ultra-relativistic case, $n \sim T^3$ increases with temperature, due to pair creation. And this increase is rapid enough that the screening length (40) *decreases* with increasing temperature. (There are more particles to participate in screening.) As a result, electric forces only operate over small distances at high temperature. Now consider a non-Abelian plasma. At zero temperature, the potential between two static test charges looks Coulomb (α/r) at very short distances [with a running $\alpha = \alpha(r^{-1})$], but is confining (linear in r) at large distances. But the fact that Debye screening only allows electric forces to operate over small distances in the limit of high, ultra-relativistic temperatures means that, if the temperature is large enough, the long-distance confining behavior will be screened away.

2.5. *Magnetic fields*

We saw the Debye effect manifest in (37) as a mass m_D for the electric potential A^0 . Note that there is no similar mass for the magnetic potential \mathbf{A} in (37). This reflects the fact that, unlike electric fields, plasmas do not screen static magnetic fields. It's the reason why the Sun and the galaxy can support magnetic fields. It's the reason that magnetic forces can act over long distances and create complicated structure like solar filaments lifting off of the surface of the sun, and why there is a whole field of classical electromagnetism called magneto-hydrodynamics (MHD).

In QED plasma, there is no screening of static magnetic fields. What happens in QCD? In the absence of screening, one might wonder if ordinary confinement once again rears its head at sufficiently large distances. Maybe a QCD plasma has electric deconfinement (because of the Debye effect) but confinement of magnetic fields (because of the absence of a similar effect). This turns out to be the case, but the physics and scale of “magnetic confinement” is quite different than the more familiar confinement of zero temperature QCD at 1 fermi.

Confinement is a non-perturbative phenomenon. At what range do QCD magnetic forces become non-perturbative at high temperature? One way to investigate is to think about attempting perturbation theory and determine the generic cost of adding each additional loop, just as previously considered for scalar theory in Fig. 5. The answer is just like (28), but with λ replaced by g^2 :

$$\text{cost} \sim g^2 \times T \sum_{\nu} \int d^3p \times (\text{two propagators}) \sim \frac{g^2 T}{\text{momentum}}. \quad (41)$$

But now there is a huge difference between gauge theory and scalar theory. In scalar theory, there was an effective mass to cut off infrared momentum. In gauge theory, in the static case, there is a mass for the electric potential A^0 but not for the magnetic potential \mathbf{A} . Let's restrict attention to the contribution from $\nu = 0$ in the frequency sum in (41), for which the static case is relevant. Because there is no mass to cut off magnetic gluons in the infrared, (41) is infrared divergent. The cost $g^2 T/p$ of adding a loop becomes non-perturbative, that is $\gtrsim O(1)$, when

the momentum scale in (41) is $p \lesssim g^2 T$. The scale of non-perturbative magnetic physics is therefore

$$p_{\text{mag}} \sim g^2 T. \quad (42)$$

The origin of this non-perturbative physics is just like that for the simple quantum-mechanical example I gave back in Sec. 1.1.1.

I have referred to the non-perturbative magnetic physics as magnetic “confinement.” Why do I call it confinement? To explain, it will be helpful to first discuss a little more formalism.

2.5.1. Imaginary-time dimensional reduction

For simplicity, let’s return for the moment to scalar theory. Consider the imaginary time action

$$S_E = \int_0^\beta d\tau \int d^3x [(\partial\Phi)^2 + \lambda\Phi^4] \quad (43)$$

at finite temperature, where I’ve assumed the temperature is high enough that I can ignore the zero-temperature mass term. This action is integrated over a slab of Euclidean space that is spatially infinite but extends only for β in the time direction, with periodic boundary conditions. In the limit of higher and higher temperature, this slab is very thin and looks more and more three-dimensional. Imagine looking at the slab with blurred eyes, so that you can only resolve physics on distance scales large compared to β . You would then be unable to tell the difference between a slab of thickness β and one of thickness zero. That is, the effective theory which described long distance physics (distances $\gg \beta$) is a *three*-dimensional Euclidean field theory.

A naive version of this is to formulate the three-dimensional version by considering only static modes above, so that $\Phi(\tau, x) \rightarrow \Phi(x)$. That is, the dynamics of the tiny imaginary time direction decouples if we look at long-distance physics.^f The $d\tau$ integral in (43) then becomes trivial, giving a factor of β , so that

$$S_E \rightarrow S_3 = \beta \int d^3x [(\nabla\Phi)^2 + \lambda\Phi^4] = \int d^3x [(\nabla\phi)^2 + \lambda T\phi^4], \quad (44)$$

where I’ve defined $\phi \equiv \beta^{1/2}\Phi$ just to give the kinetic term of the three-dimensional theory a conventional normalization.

In more detail, saying that the imaginary time dynamics decouples is not quite the same as saying it has no effect: it can give finite renormalizations to the interactions of static modes when one integrates out the non-static ($\nu_n \neq 0$) modes of the field. In particular, consider the contribution to the one-loop self-energy diagram of Fig. 3 when the external lines are static ($\nu = 0$) but the internal line is summed over the non-static ($\nu_n \neq 0$) modes which are decoupling. This contribution turns

^fjust like excited Kaluza-Klein modes decouple in a theory with tiny, compact extra dimensions.

out to give the $\#\lambda T^2$ thermal contribution to m_{eff}^2 that we have discussed earlier. So, the decoupling imaginary time dynamics contributes to give an effective mass in the long-distance three-dimensional effective theory of

$$m_3^2 = m_0^2 + \#\lambda T^2. \quad (45)$$

This is the most important effect. There are also sub-leading effects on the coupling $\lambda_3 \simeq \lambda T$ of the three-dimensional theory and the generation of sub-leading higher-dimensional interactions, such as $\nu_3 \phi^6$ with $\nu_3 \sim \lambda^3$. Perturbative calculations can be done to determine all the coefficients of interest in the effective theory, and such imaginary-time “matching calculations” are a mature, well-understood technology.

What happens if we ask the same question about gauge theory? If we do naive dimensional reduction, the 4-dimensional action at high temperature

$$S_{\text{E}} = \int_0^{\hbar\beta} d\tau \int d^3x F^2 \quad (46)$$

reduces to

$$S_{\text{E}} = \beta \int d^3x F^2, \quad (47)$$

and the β can again be absorbed by a field redefinition, making the three-dimensional coupling $g_3^2 = g^2 T$. Ignore A^0 for a moment. The moral is then that the effective long-distance (i.e. low-momentum) theory for high temperature four-dimensional gauge theory is (zero temperature) *three*-dimensional gauge theory, with the scale set by $g^2 T$. The question about whether the long-distance physics is confining is then a question about whether three-dimensional non-abelian Yang-Mills is confining. The answer (from lattice simulations) turns out to be that it is.^g

It’s interesting to put explicit \hbar ’s back into this discussion. The dimensional reduction is then

$$\frac{S_{\text{E}}}{\hbar} = \hbar^{-1} \int_0^{\hbar\beta} d\tau \int d^3x F^2 \rightarrow \hbar^{-1} \times \hbar\beta \int d^3x F^2 = \beta \int d^3x F^2, \quad (48)$$

where the \hbar has to appear in the upper limit of the $d\tau$ integration by dimensional analysis if we define $\beta \equiv 1/k_{\text{B}}T$. The absence of \hbar on the far right side of (48) shows that the effective long-distance theory is a *classical* field theory, consistent with the discussion in Sec. 1.1.1 that non-perturbative physics can occur at high temperatures in weakly coupled theories but that it will be classical in nature.

^gWhat happens to the A^0 ? It picks up the Debye mass from integrating out the effects of the non-zero frequency modes. In three-dimensional language, it becomes a massive, adjoint color scalar field and, because of its mass, decouples at distances $\gg 1/m_{\text{D}} \sim 1/gT$.

2.6. Summary of Scales

We've now seen the following hierarchy of momentum scales:

- T : typical particle momenta;
- gT : Debye mass, causing charge deconfinement;
- g^2T : magnetic confinement.

The corresponding distance scales are shown in Fig. 7 .

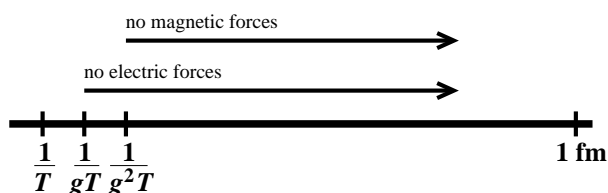


Fig. 7. A cartoon of the distance scales relevant to time-independent questions of equilibrium, high-temperature gauge theory.

3. Dynamics Near Equilibrium: Plasma Waves

For ω and k both small compared to T , I previously asserted that the gauge boson self-energy has the form $\Pi_{\mu\nu}(\omega, k) = g^2 T^2 f_{\mu\nu}(\omega/k)$. So far, I have only discussed the static limit $\omega = 0$ (applying to $\omega \ll k \ll T$), where the self-energy was given by (37). Let's now consider the opposite limit $k = 0$ (applying to $k \ll \omega \ll T$). This is not a natural limit in the imaginary-time formalism, where $\omega = i\nu_n = 2\pi nT$. Imaginary frequencies cannot be simultaneously non-zero and small compared to T . But one can find the desired result by appropriate analytic continuation. It turns out to give^{10,13}

$$\Pi_{\nu}^{\mu} = m_{\text{D}}^2 \begin{pmatrix} 0 & & & \\ & \frac{1}{3} & & \\ & & \frac{1}{3} & \\ & & & \frac{1}{3} \end{pmatrix}. \quad (49)$$

This generates a mass gap for low-momentum (color) electromagnetic waves propagating in the plasma:

$$m_{\text{pl}} = \frac{m_{\text{D}}}{\sqrt{3}}. \quad (50)$$

This is known as the plasma frequency. (See Jackson!¹⁴) Or, regarding plasma wave quanta, it is known as the soft plasmon mass.

A massive gauge field has a longitudinal polarization, in addition to the two transverse polarizations familiar from propagating electromagnetic waves in vacuum. The physical picture of a longitudinal plasma wave is that it is a charge wave

together with the associated electric fields. For simplicity, consider QED rather than QCD. Suppose that an equilibrium plasma is disturbed to have a small excess of charge in certain regions, as depicted in Fig. 8a (which shows only the excess charge). Electric forces will cause the charges to accelerate in the directions shown by the arrows in that figure. The charges will then move to cancel each other, except they will overshoot because of inertia, leading to the situation shown in Fig. 8b, with electric forces again shown by the arrows. The wave will oscillate between these two states (eventually dissipating because of random collisions—a subleading effect).^h

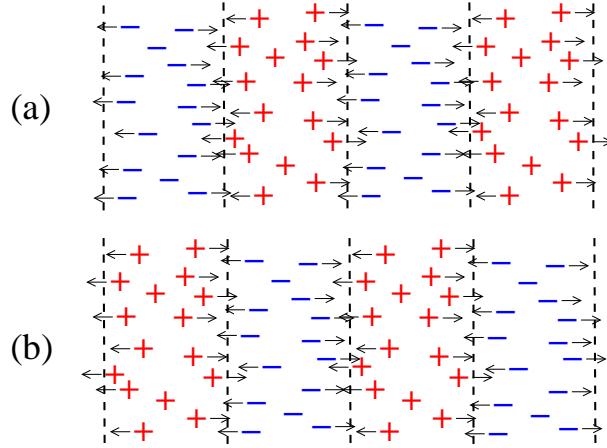


Fig. 8. A picture of a longitudinally polarized plasma wave as oscillations between (a) and (b).

In general, the dispersion relation for propagating gluons in the plasma has a complicated form but two simple limiting cases:

$$k \ll m_{\text{pl}} : \quad \omega^2 \simeq k^2 + m_{\text{pl}}^2 \quad (\text{transverse, longitudinal}) \quad (51)$$

$$k \gg m_{\text{pl}} : \quad \omega^2 \simeq k^2 + \frac{1}{2}m_{\text{pl}}^2 \quad (\text{transverse}) \quad (52)$$

The first case is the one just discussed, which we'll call the soft gluon case. The second case says that “hard” gluons have a mass of $m_\infty \equiv m_{\text{pl}}/\sqrt{2} = m_{\text{D}}/\sqrt{6} \sim gT$.

Fermions get similar masses of order gT from medium effects on their propagation. The moral is that, at very high temperature, all propagating (quasi-)particles get masses of order gT .

^hNote that ultra-relativistic particles move at nearly the speed of light and so do not simply stop and turn around. Moreover, my discussion of the self-energy Π has been perturbative, and small, perturbative fields can only have small effects on the otherwise straight-line trajectories of the particles. These small deviations, however, can slightly increase the density of one charge type in one place and decrease it in another. Fig. 8 should be considered a particle-averaged picture of local charge fluctuations, rather than a description of the motion of each individual particle.

This might seem contradictory. If all propagating particles have masses of order gT , then what were those “massless” low-momentum ($k \sim g^2T$) gluons that I said caused magnetic confinement? They came from the spatial polarizations of the $\omega = 0$ ($\omega \ll k \ll T$) self-energy (37). They are not independently propagating excitations because they have *space*-like ($\omega < k$) momenta. What they represent are not propagating particles themselves (which have time-like momenta) but the magnetic fields created by those moving particles.

4. Dynamics Near Equilibrium: Relaxation and Viscosity

Previously, I have emphasized the use of imaginary time path integrals in understanding various static aspects of thermal equilibrium. If one is studying static properties (the equation of state, equal-time correlation functions, and so forth), it doesn't matter whether one works in imaginary time or real time. And some things, like magnetic confinement, are easiest to see and understand in the imaginary time formalism. For static quantities, the imaginary time formalism, dimensional reduction, and perturbative matching calculations have provided a systematic, mature technology for studying problems order by order in small coupling.

In contrast, there are many time-dependent aspects of plasmas (such as viscosity, electrical conductivity, and other quantities characterizing relaxation) where it is a struggle to get even leading-order results. Organizing small-coupling calculations in some more useful way than the traditional loop expansion turns out to be really important, as exemplified by Fig. 9. This figure depicts just one of an infinite set of diagrams that contributes to the *leading*-order result for the shear viscosity. (Actually, there is an obvious error in the diagram which I have not corrected. Can you spot it?¹)

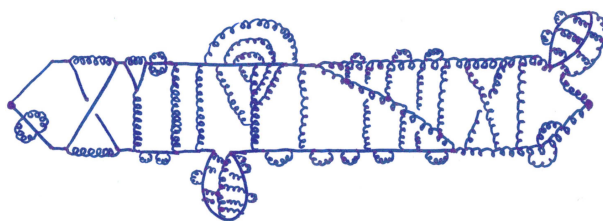


Fig. 9. One of an infinite class of graphs contributing to the QCD shear viscosity at leading-order (except for an obvious error).

Indeed, there are basic aspects of the dynamics of plasmas which are incredibly difficult to see in imaginary time.

¹Answer: The long diagonal gluon line was meant to be a quark line. There is no such thing as a quark-gluon-gluon vertex.

4.1. A failure of imaginary-time intuition

For simplicity, let's return to scalar theory. In Sec. 2.5.1, we learned that the long-distance effective theory is a three-dimensional theory

$$S_3 = \int d^3x [(\nabla\phi)^2 + m_3^2\phi^2 + \lambda_3\phi^4 + \dots] \quad (53)$$

where $\phi \simeq \beta^{1/2}\Phi$, $m_3^2 \simeq m_0^2 + \#\lambda T^2$, and $\lambda_3 \simeq \lambda T$. There is a non-zero effective mass m_3 in this theory. Technically, this means that if we evaluate equal-time correlators, we'll find that they fall exponentially at large distances:

$$\langle \phi(0, \mathbf{x}) \phi(0, \mathbf{y}) \rangle \sim e^{-m_3|\mathbf{x}-\mathbf{y}|}. \quad (54)$$

The presence of a mass in the above low-momentum effective theory might make you think that there is a minimal energy m_3 for creating excitations of the system. This would be wrong. At finite temperature, there are always long wavelength, low frequency oscillations in the form of sound waves, such as depicted (for an ultra-relativistic theory) in Fig. 10. A sound wave is a pressure wave. Higher pressure means higher energy and so, in the ultra-relativistic limit, higher particle density (because of pair creation). So, in the cartoon of Fig. 10, I've indicated regions of higher pressure by drawing more particles. If the wavelength is long, the period of oscillation has to be long, because energy is conserved: the only way that high and low energy regions can swap places is for energy to be transferred over distances of order a wavelength, and the rate of such transfer is limited at the very least by the speed of light. In general, a sound wave has

$$\omega \simeq v_s k \rightarrow 0 \quad \text{as} \quad k \rightarrow 0, \quad (55)$$

where v_s is the speed of sound.

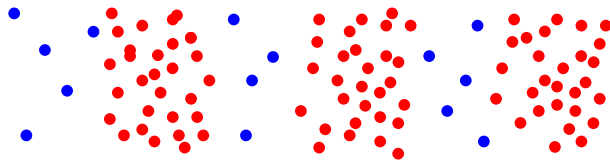


Fig. 10. A cartoon of a sound wave in an ultra-relativistic gas.

So what was wrong with thinking that the mass m_3 in the three-dimensional effective theory implied an energy gap (and so minimum frequency) for excitations? This is a problem of thinking too much in imaginary time. The three-dimensional high-temperature effective theory is an effective theory of low-momentum *static* physics ($\omega = 0$ and $k \ll T$). But sound waves have $\omega \sim k \ll T$.

4.2. A sequence of real-time effective theories

Sound waves are an example of a hydrodynamic phenomenon. In general, if I am interested in the real-time physics of a finite temperature system at long enough distance and time scales, I can describe the system using hydrodynamics. Over long time scales, the only excitations that will not have decayed away are long wavelength variations in locally conserved quantities, such as energy and momentum density. (Because of conservation, these quantities can only change as fast as they can move from one place to another, as I just described for sound.) The effective theory of such quantities is hydrodynamics.^j

What if we want to compute, from first principles, parameters of the hydrodynamic description, such as viscosity (to be reviewed shortly)? It turns out it's somewhat overwhelmingly complicated to jump in a single step from the microscopic description in terms of quantum field theory to the macroscopic description in terms of hydrodynamics. Diagrams like Fig. 9 are involved. What's needed is to organize the calculation by stepping first through another effective theory at intermediate (and longer) scales. That modern, state-of-the-art effective theory was just invented... in 1872, by some fellow named Boltzmann. It is kinetic theory.

4.2.1. The form of the Boltzmann equation

In kinetic theory, one describes the state of the system in terms of a classical phase space density of particles, $f(\mathbf{x}, \mathbf{p}, t)$. The basic equation of kinetic theory is simply the statement that (in the absence of external forces) changes in momentum \mathbf{p} only occur by loss or gain through scattering:

$$\frac{df_{\mathbf{p}}}{dt} = -(\text{loss})_{\mathbf{p}} + (\text{gain})_{\mathbf{p}}. \quad (56)$$

For example, schematically,

$$\frac{\partial f}{\partial t} + \frac{\partial \mathbf{x}}{\partial t} \cdot \frac{\partial f}{\partial \mathbf{x}} = - \left| \begin{array}{cc} \mathbf{p} & \mathbf{p}' \\ \mathbf{k} & \mathbf{k}' \end{array} \right|^2 + \left| \begin{array}{cc} \mathbf{p}' & \mathbf{p} \\ \mathbf{k}' & \mathbf{k} \end{array} \right|^2. \quad (57)$$

Here, I've just used the chain rule on the left-hand side. I've represented the loss and gain terms on the right-hand side by the leading-order diagrams (squared to give rates) for losing or creating a particle of momentum \mathbf{p} . I've suppressed details of phase space integrals, the density of particles to scatter off of, or final state Bose enhancement factors (or Pauli blocking factors for fermions). If I put all that in, and use crossing symmetry to equate the gain and loss diagrams, we get the Boltzmann equation:

$$(\partial_t + \mathbf{v} \cdot \nabla)f = -C[f], \quad (58a)$$

^jA nice place to very quickly pick up the basics of non-relativistic hydrodynamics is chapters 41–42 of the Feynman lectures, volume 2.¹⁵ For relativistic hydro, try Weinberg.¹⁶

where the “collision term” is

$$C[f] = \int_{\mathbf{k}\mathbf{p}'\mathbf{k}'} \left| \begin{array}{c} \mathbf{p} \\ \mathbf{k} \end{array} \times \begin{array}{c} \mathbf{p}' \\ \mathbf{k}' \end{array} \right|^2 \left\{ f_{\mathbf{p}} f_{\mathbf{k}} (1 \pm f_{\mathbf{p}'}) (1 \pm f_{\mathbf{k}'}) - f_{\mathbf{p}'} f_{\mathbf{k}'} (1 \pm f_{\mathbf{p}}) (1 \pm f_{\mathbf{k}}) \right\} + (\text{all other scattering processes}). \quad (58b)$$

The left-hand side of (58a) is called the convective derivative of f . If there were no collisions, it would simply reflect the fact that f at a particular point \mathbf{x} can change with time simply because the particles’ velocities move them to another point $\mathbf{x} + \mathbf{v}\Delta t$.

4.3. Shear viscosity η in scalar theory

As an example of how things work, I’ll start with the example of shear viscosity in scalar ϕ^4 theory. I’ll start by describing what shear viscosity is. One way to think of it is to imagine a moving stream (infinitely long but finite radius R) surrounded by a stationary ocean. If we wait, the stream will broaden and slow down, eventually dissipating its momentum across the bulk of the ocean. The shear viscosity η characterizes the rate of this dissipation, which is proportional^k to η/R^2 .

How does the dissipation happen? At finite temperature, particles (of water, air, quark-gluon plasma, whatever) are bouncing around in all directions. In the stream, the *average* value of the component of momentum in the stream’s direction is non-zero. If we wait long enough, the particles in the stream will randomly bounce out of the stream, spreading this net momentum into the bulk of the medium. Because of collisions, the particles move transversely in a drunken, random walk, as in Fig. 11. The shorter the steps of that walk (the shorter the mean free path), the harder it will be to get out. Note also that the more momentum each particle carries, the more it will transfer when it does get out. Roughly speaking,

$$\text{rate} \propto \eta \sim (\text{mean free path}) \times (\text{energy-momentum density}). \quad (59)$$

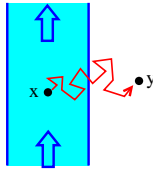


Fig. 11. A particle random walking out of a stream of moving fluid.

How could we measure all of this formally? Energy and momentum are measured by the stress-energy tensor $T_{\mu\nu}$. Imagine applying the operator $T_{\mu\nu}(x)$ to the

^kMore specifically, η is defined so the rate $\sim \eta/R^2(\epsilon + P)$ where ϵ and P are the energy density and pressure. In the non-relativistic limit, $\epsilon + P$ becomes mass density.

equilibrium state in order to create a disturbance at a space-time point x in the equilibrium fluid. Now we can later measure $T_{\mu\nu}(y)$ at other points y to see how the disturbance is spreading out with time. So, it turns out to be possible to relate viscosity to knowledge of the low-momentum behavior of the (retarded) stress-energy correlator.¹ We can then imagine computing such correlators using diagrammatic methods of (finite temperature) quantum field theory. Fig. 12a shows an infinite class of diagrams which contribute to the leading-order results for shear viscosity in ϕ^4 theory. Why are there so many interaction vertices? One can get a rough idea by considering chopping the diagram in half, with the upper half shown in Fig. 12b. This looks just like the random walk depicted in Fig. 11 of a particle from x to y undergoing many collisions with other particles on its way out. If we're interested in long-wavelength, long-time behavior, which is what viscosity (and hydrodynamics in general) characterizes, then the number of collisions involved is unavoidably large.

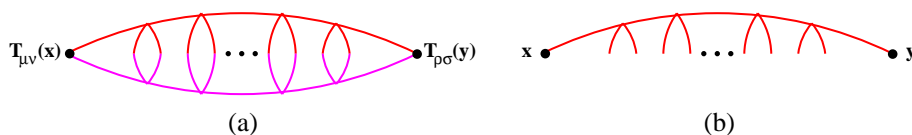


Fig. 12. (a) A set of Feynman diagrams contributing to leading-order shear viscosity, and (b) a cut of those diagrams.

Fig. 12b is an amplitude, and we must square it to get a rate. One can crudely think of the bottom half of Fig. 12a as the conjugate amplitude.

There's a slight variation needed to get *all* the diagrams that contribute to the leading-order shear viscosity, and I just want to give you a flavor of it without dwelling on details. In the multiple scattering depicted by Fig. 12b, we should think of the intermediate lines as being on-shell: the particle is on-shell in between successive independent collisions. But that means the propagators corresponding to those lines are infinite. This is a standard problem in quantum mechanics whenever you produce a state that does not live forever. A standard example in zero-temperature quantum field theory is the production of an unstable particle. There the physics which saves the day and avoids the on-shell divergence is the finite width of the unstable state, which replaces

$$\frac{1}{P^2 - M^2} \rightarrow \frac{1}{P^2 - M^2 - iM\Gamma} \quad (60)$$

and generates a Breit-Wigner form. At finite temperature, even stable particles have a width, because collisions with other particles will eventually knock them out of the momentum state they are in. That width is related to the imaginary part of

¹This and similar relations are known as Kubo relations.

the self-energy, which first arises in two-loop self-energy diagrams (the imaginary part corresponding to the rate for leading-order $2 \rightarrow 2$ scattering). One can effect the substitution analogous to (60) by resumming these two-loop self-energies into the particle's propagator, and so the relevant diagrams for the leading-order shear viscosity are actually those shown in Fig. 13.

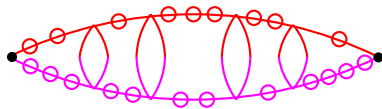


Fig. 13. The leading-order diagrams for shear viscosity at high temperature in ϕ^4 theory.

In the context of ϕ^4 theory, this diagrammatics was worked out by Jeon in 1995.¹⁷ He showed that the leading-order contribution of adding up the diagrams of Fig. 13 was completely equivalent to finding the viscosity by linearizing the Boltzmann equation (58) in small fluctuations about equilibrium, and then solving those linearized equations. The Boltzmann equation approach is a lot easier than analyzing diagrams. In either case, the result is $\eta \simeq 2860 T^3/\lambda^2$.

4.4. Validity of the Boltzmann equation

Why does the Boltzmann equation work? There are two important conditions for its validity.

The first condition is that the de Broglie wavelengths of particles must be small compared to the mean free path between collisions for the relevant particles:

$$\lambda(\text{de Broglie}) \ll \text{mean free path}. \quad (61)$$

This allows one to treat the particles as *classical* particles between collisions (allowing \mathbf{x} and \mathbf{p} to be treated as independent, classical variables in the Boltzmann equation). For scalar theory, the typical particle momentum is order T , and so the de Broglie wavelengths are of order $1/T$. The leading-order $2 \rightarrow 2$ scattering amplitude is proportional to λ , rates are therefore proportional to λ^2 , and so, by dimensional analysis, the mean free path is of order $1/\lambda^2 T$. The condition (61) is thus satisfied in the weak-coupling limit.

The second requirement is that the quantum-mechanical duration of individual scattering events should be small compared to the mean free time between collisions:

$$\text{scattering duration} \ll \text{mean free time}. \quad (62)$$

Otherwise, there would be quantum interference between successive scatterings, and we could not treat the scatterings as independent. For scalar theory, the leading-order scattering diagram shown in (58b) is a point interaction, which has zero time duration, and so this is not an issue.

The difficulty, as we'll eventually see, is that the second condition *fails* for gauge theories! That means we'll have to work a little bit harder.

4.5. Boltzmann for Gauge Theories

Why can't we do what we did for scalar theory, putting the leading-order scattering processes into the collision term? Why isn't the Boltzmann equation for gauge theory schematically of the form

$$(\partial_t + \mathbf{v} \cdot \nabla)f = \left| \text{diagram} \right|^2 + (\text{other leading-order } 2 \rightarrow 2 \text{ diagrams})? \quad (63)$$


Before we can understand the problem, we will have to discuss some basic scales associated with the process of Coulomb scattering depicted in (63).

By the way, in general I will use straight lines in diagrams to represent any $p \sim T$ particle. So the diagram shown explicitly in (63) represents gg and gq processes as well as qq processes (and processes involving anti-quarks).

4.5.1. Coulomb scattering basics

In vacuum, Coulomb scattering has an infinite cross-section, arising from an infrared divergence associated with the long-range nature of the Coulomb force. The diagram in (63) is proportional to g^2/Q^2 , where Q is the exchanged 4-momentum and $1/Q^2$ comes from the corresponding propagator. After squaring the amplitude and integrating over the final state phase space, one finds that the cross-section is of order

$$\sigma \sim \int d(Q^2) \left| \frac{g^2}{Q^2} \right|^2, \quad (64)$$

which is infrared divergent. In a plasma, however, the momentum exchange is cut off in the infrared by Debye screening at $Q \sim m_D$. So (with a caveat discussed later), the cross-section (64) is

$$\sigma \sim \frac{g^4}{m_D^2} \sim \frac{g^4}{(gT)^2} \sim \frac{g^2}{T^2}. \quad (65)$$

Here's an intuitive way to the same result which I find provides a quick way to remember how things work. Consider a particle moving through the medium, and let the term "scatterer" refer to another particle that it scatters from. The Coulomb field of the scatterer extends out to the Debye screening length ξ_D . The cross-sectional area of that region of space is $\sim \xi_D^2$. If interactions were not weak, then the scattering cross-section would also be $\sim \xi_D^2$ (like scattering off of a hard sphere). But, in weak coupling, the leading-order diagram of (63) has two explicit powers of g , which gives g^4 in the rate. So this modifies ξ_D^2 to

$$\sigma \sim g^4 \xi_D^2, \quad (66)$$

which is the same as (65).

With the cross-section in hand, we can find the mean-free time τ between collisions. The rate τ^{-1} for a given particle to collide is proportional to the cross-section

σ , the density $n \sim T^3$ of scatterers, and the relative velocity $v \sim 1$ that the particle moves through those scatterers. So

$$\tau \sim (n\sigma v)^{-1} \sim (T^3\sigma)^{-1}. \quad (67)$$

Using (65),

$$\tau \sim \frac{1}{g^2 T}. \quad (68)$$

The quantum duration of this scattering event is of order $1/Q \sim 1/m_D \sim 1/gT$. For weak coupling, this duration is indeed small compared to the mean free time (68). So far, there is no problem with condition (62) for the validity of the Boltzmann equation.

Typical Coulomb scatterings do not significantly randomize a particle's direction and so individually do not create the random walk depicted in Fig. 11. To see this, let's estimate the angle of deflection for a typical Coulomb scattering. The momentum transfer of order $Q \sim m_D$ will not significantly change the total momentum $p \sim T$ of a typical plasma particle, but it will give a transverse kick to that momentum of order $p_\perp \sim m_D$. That leads to a change in direction of order

$$\Delta\theta \sim \frac{p_\perp}{p} \sim \frac{m_D}{T} \sim g, \quad (69)$$

which is small in the weak-coupling limit.

Much more rarely, individual Coulomb collisions will have large momentum transfers, or equivalently small impact parameters, producing large angle deflections $\Delta\theta \sim 1$ and $p_\perp \sim p$. This comes from the range of integration $Q^2 \sim p^2$ in (64), corresponding to $\sigma \sim g^4/p^2 \sim g^4/T^2$. Equivalently, it comes from impact parameters b of order $1/p$, leading to $\sigma \sim g^4 b^2 \sim g^4/p^2$. Computing $\tau \sim (n\sigma v)^{-1}$, we can summarize this and the previous result as

$$\tau \sim \begin{cases} 1/g^4 T, & \text{for } \Delta\theta \sim 1; \\ 1/g^2 T, & \text{for } \Delta\theta \sim g; \end{cases} \quad (70)$$

A picture is shown in Fig. 14.

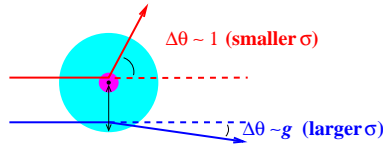


Fig. 14. A picture of typical small-angle, large-impact parameter Coulomb scattering vs. rarer large-angle, small-impact parameter scattering.

So which sort of Coulomb collisions matter for characterizing the random walk that determines shear viscosity? The answer is that they both do. The mean free

time $\tau \sim 1/g^4 T$ for a single large-angle collision is the same as the time $N/g^2 T$ for a large number $N \sim 1/g^2$ of small-angle collisions (each $\delta\theta \sim g$). The small-angle collisions will cause a random walk in the deflection angle. So the total deflection grows as \sqrt{N} , giving

$$\Delta\theta \sim g\sqrt{N} \sim 1. \quad (71)$$

So, as summarized in Fig. 15, a typical plasma particle's direction gets randomized in a time of order $\tau \sim 1/g^4 T$, whether it be by a single large-angle scattering or a sequence of many small-angle scatterings.^m

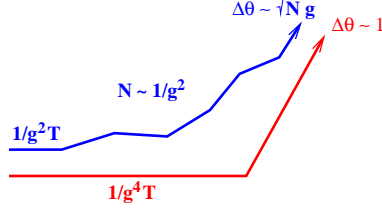


Fig. 15. Different ways to get a large-angle scattering in time $\sim 1/g^4 T$.

4.5.2. Showering

We have seen that the relevant time scale for the random walk in particle velocities is

$$\tau_{\text{random}} \sim \frac{1}{g^4 T}. \quad (72)$$

This is known as the “transport” mean free path. Does anything *else* happen on this time scale that might be relevant? The answer is showering, by which I mean hard, nearly collinear bremsstrahlung from small-angle collisions, such as shown in Fig. 16. Emitting the extra bremsstrahlung gluon costs an extra factor of g^2 compared to the small-angle $2 \rightarrow 2$ scattering rate $\sigma_{2 \rightarrow 2} \sim 1/g^2 T$ of the previous section. That

^mThroughout this discussion, I have talked about Coulomb scattering and the fact that Coulomb fields are Debye screened. But why can't $2 \rightarrow 2$ scattering occur via magnetic forces, which can operate over scales as large as the magnetic confinement scale $\xi_M \sim 1/g^2 T$? One might guess the cross-section for such super-large impact parameter scatterings to be $\sigma \sim g^4 \xi_M^2 \sim 1/T^2$, which is much larger than the other cross-sections discussed, and the deflection to be $\Delta\theta \sim p_{\perp}/p \sim \xi_M/T \sim g^2$. But it turns out that the cross-section estimate is wrong. It's true that *static* magnetic fields are not screened at the scale $1/gT$, but changing magnetic fields can be. This is Lenz's Law from freshman physics: conductors resist changes to magnetic fields. (The changing B fields produce E fields, which are in turn screened.) This suppression produces $\sigma \sim (g^2/T^2) \ln(m_D/g^2 T)$, and the result is that $\Delta\theta \sim g^2$ collisions are no more frequent than $\Delta\theta \sim g$ collisions and so are not important in terms of randomizing particle directions.

means the rate is g^2 times smaller, and so the mean free path for showering is $1/g^2$ times bigger:

$$\tau_{\text{shower}} \sim \frac{1}{g^2} \tau_{2 \rightarrow 2} \sim \frac{1}{g^2} \frac{1}{g^2 T} \sim \frac{1}{g^4 T}. \quad (73)$$

That is the same order as the transport mean free path (72).

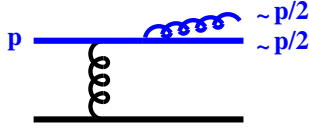


Fig. 16. Showering of a particle by hard, nearly-collinear bremsstrahlung during a small-angle $2 \rightarrow 2$ scattering.

You might wonder why it’s relevant whether or not the particle splits into two. The point of our discussion of shear viscosity is to understand how quickly momentum can be transported out of the stream of fluid in Fig. 11. After a nearly-collinear split like Fig. 16, the same total amount of momentum is still flowing in roughly the same direction as it was before the collision. So how can this process impede momentum flow and so affect the shear viscosity? The answer is that the original momentum p is now carried by two particles with lesser momentum, and it is easier for subsequent Coulomb scatterings to deflect the directions of lower-momentum particles. The deflection angle $\Delta\theta \sim p_{\perp}/p \sim m_D/p$ of a typical Coulomb scattering will be larger if p is smaller. So showering has this indirect effect on momentum transport, which must be taken into account in a complete leading-order treatment.

We might hope to include this physics into our Boltzmann equation as (schematically)

$$(\partial_t + \mathbf{v} \cdot \nabla)f = \left| \begin{array}{c} \diagup \\ \text{gluon} \\ \diagdown \end{array} \right|^2 + \left| \begin{array}{c} \text{gluon} \\ \text{---} \\ \text{gluon} \end{array} \right|^2. \quad (74)$$

It turns out, however, that the internal straight line in Fig. 16 is only off-shell by a very tiny amount, and this has unfortunate consequences for the quantum mechanical duration of the bremsstrahlung process. The splitting of one massless particle into two exactly collinear massless particles is allowed by energy and momentum conservation, which would allow the internal line to be exactly on shell. Our particles are not massless: they have small thermal masses of order gT , and so they require a small injection of momentum to split. It turns out that the internal straight line in Fig. 16 is off-shell by an amount $\Delta E \sim m_{\infty}^2/p \sim g^2 T$ in energy. This means that the scattering duration, known in this context as the “formation time” of the bremsstrahlung gluon, is

$$\text{formation time} \sim \frac{1}{\Delta E} \sim \frac{1}{g^2 T}. \quad (75)$$

But this is parametrically the same as the mean free time $\tau_{2 \rightarrow 2} \sim 1/g^2 T$ between small-angle scatterings! We have included a process that fails the condition (62) that scattering durations be small compared to mean free times between collisions, and so a Boltzmann treatment of the two processes in (74) is not valid.¹¹

4.5.3. The Landau-Pomeranchuk-Migdal effect

To deal with this situation, we have to leap from the physics of 1872 to the truly cutting-edge physics of... 1955. We have been discussing QCD and quark-gluon plasmas, but the same issues apply to QED and the electromagnetic showering of very-high-energy cosmic rays in the atmosphere. Consider a high-energy electron scattering off of the Coulomb field of a nucleus and emitting a hard, bremsstrahlung photon. It was noted that, at sufficiently high energy, the formation time would exceed the mean free path between collisions in the atmosphere. The result is a suppression of the rate for bremsstrahlung, because the bremsstrahlung photon effectively sees only one net deflection of the charged particle during its formation time, rather than the several individual deflections associated with each individual scattering. This is known as the Landau-Pomeranchuk-Migdal (LPM) effect.¹⁸

How can we proceed? The long formation time means that photon production associated with one collision could have interference effects with photon production associated with a later collision. In terms of diagrams, there could be interference terms between photon production (i) just before and (ii) just after some set of N consecutive scatterings, as shown on the right-hand side of Fig. 17. We want to sum up all these possibilities into an effective rate for particle splitting in the medium, depicted by the left-hand side of Fig. 17.

It turns out (without going into details) to be useful to imagine gluing together the diagrams for the amplitudes and conjugate amplitudes to rewrite the right-hand side of Fig. 17 in the form of a sum of diagrams of the form of Fig. 18 (vaguely analogous to what happened in Fig. 12). Before I explain why it's useful, I'll first discuss the generalization from QED to QCD.

The effective Boltzmann equation for QCD, which fixes the LPM problem by using an effective splitting rate that sums up the interferences, is schematically of

¹¹I should be a little careful to distinguish matters of principal from matters of practicality. One can imagine that the formation time might be numerically small compared to $\tau_{2 \rightarrow 2}$ even if not suppressed by a power of g . If so, one might get a quite reasonable numerical approximation to the exact weak-coupling result by ignoring the problem. This turns out to be the case for shear viscosity. But I continue nonetheless to discuss what's needed for a complete leading-order calculation because it highlights physics that is important to other matters, such as the penetration of high energy jets through a thermal medium.

$$\left| \text{---} \text{---} \text{---} \right|^2 = \left| \text{---} \text{---} \text{---} \right|^2 + \left(\text{---} \text{---} \text{---} \right)^* \left(\text{---} \text{---} \text{---} \right) + \left(\text{---} \text{---} \text{---} \right)^* \left(\text{---} \text{---} \text{---} \right) + \dots$$

Fig. 17. The effective splitting rate in QED as a sum over possible interferences of photon emission before or after a certain number of scatterings. Here, the crosses represent the sources for the scattering electromagnetic fields, such as fixed nuclei in the case of high-energy air showers.

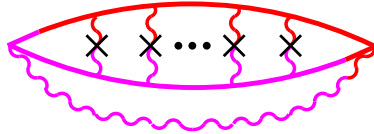


Fig. 18. Another representation of the right-hand side of Fig. 17.

the form^{19,20,o,p}

$$(\partial_t + \mathbf{v} \cdot \nabla) f = \left| \text{---} \text{---} \text{---} \right|^2 + \left| \text{---} \text{---} \text{---} \right|^2. \tag{76}$$

The difference of the last term with the QED case of Fig. 17 is that the bremsstrahlung gluon carries color and so can also scatter from the medium. In addition, there can be final state interactions between the two split particles. Fig. 19 shows a typical interference term, along with the diagrammatic representation if you sew together the amplitude and conjugate amplitude, analogous to Fig. 18.^q

$$\left(\text{---} \text{---} \text{---} \right)^* \left(\text{---} \text{---} \text{---} \right) = \text{---} \text{---} \text{---}$$

Fig. 19. A sample interference term for the LPM effect in QCD, analogous to terms in Figs. 17 and 18.

^oThe last term in (76) should be understood to include all $1 \leftrightarrow 2$ splittings, such as $q \leftrightarrow qg$, $g \leftrightarrow gg$, and $g \leftrightarrow q\bar{q}$.

^pOne can wonder if this equation double counts some small-angle collisions, because small-angle collisions appear both in the effective splitting rate and explicitly as the first diagram in (76). The answer is yes but it's okay at leading-order, because only a parametrically small fraction $t_{\text{form}}/t_{\text{random}} \sim g^2$ of small-angle collisions take place while a bremsstrahlung gluon is forming.

^qFor a discussion in the language used here, see Ref. 21. For earlier work, see Ref. 22.

I haven't given you any details about how exactly you are supposed to evaluate a diagram like the right-hand side of Fig. 19. And I have to sum up an infinite class of similar diagrams, which sounds difficult. But, having written the diagrams in this form, I can now explain to you how the problem of doing this entire diagram sum can be reduced to the problem of solving an integral equation (which in practice can be done numerically⁴). In Fig. 20, the left-hand side represents the infinite sum of diagrams needed for the LPM effect. On the right-hand side, the blob represents the sum of those same diagrams if I simply cut out their left vertex. This blob satisfies an integral equation shown by the first line in Fig. 21, which you can see by thinking of all but the first line term on the right-hand side as a "perturbation" and then solving the equation iteratively. Fig. 21 is an integral equation because there is one loop integral, in terms of the unknown blob, on all but the first term on the right-hand side.

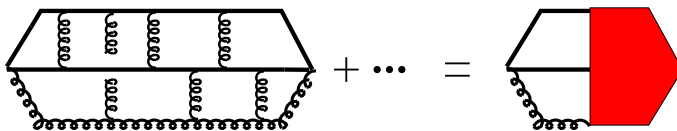


Fig. 20. Rewriting the sum of QCD LPM graphs in terms of an unknown blob.

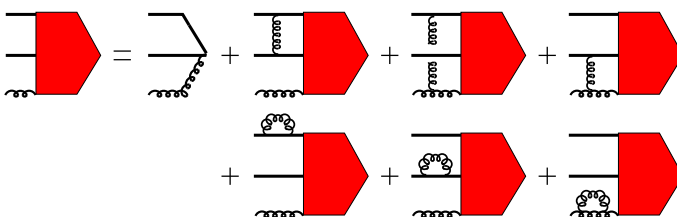


Fig. 21. An integral equation for the blob.

You'll see, however, that in Fig. 21 I have also included a second line which sums in some corresponding self-energy corrections. That's because I've hidden something from you in the interest of simplifying my presentation so far. For the same reason that I needed to include the imaginary part of self-energy diagrams in Fig. 13, I need to do it here.^f Finally, I should mention that all the lines shown explicitly in Fig. 21 are themselves resummed with $O(g^2 T^2)$ one-loop self-energies (which give Debye screening and whose imaginary parts give the little circular loops

^fWhen a particle propagates over a time as long as its mean free path, I can't ignore the effect of its width on the propagator.

representing the scatterers on the right-hand side of Fig. 19, which I am no longer showing explicitly).

4.5.4. *Result for shear viscosity*

I should quote you a result just to show that all of this formalism can be successfully implemented. We’ve previously discussed (59) that shear viscosity is proportional to the mean free time (72) characteristic of a particle’s random walk. The rest is just factors of T determined by dimensional analysis, giving $\eta \sim T^4 \tau_{\text{random}}$. So we expect $\eta \simeq \# T^3 / g^4$, and we’d like to know the numerical coefficient $\#$, analogous to the result quoted earlier for scalar theory.

However, it’s slightly more complicated than that. The reason is because of the multiple ways for a particle’s velocity to randomize, as was depicted in Fig. 15. Both large and small angle collisions were equally efficient. So is a sequence of intermediate angle collisions. As a result, the rate is enhanced by a logarithm, known as the “Coulomb log,”^s counting all the decades of possibility between “large angles” ($\delta\theta \sim 1$) and “small angles” ($\delta\theta \sim g$), so that

$$\tau_{\text{random}} \sim \frac{1}{g^4 T \ln(1/g)} \quad \text{and} \quad \eta \sim \frac{\# T^3}{g^4 \ln(1/g)}. \quad (77)$$

But logarithms are not particularly big, and there are corrections to this formal limit order by order in $1/\ln(1/g)$. So, if one wants a result good to the leading *power* of g , it has the functional form

$$\eta \simeq \frac{T^3}{g^4 \ln(1/g)} F(\ln(1/g)), \quad (78)$$

and the answer requires giving a logarithmically-sensitive function F rather than a single numerical coefficient $\#$. Just to prove to you that it can be done, Fig. 22 shows the leading-order result of the ratio of shear viscosity η to entropy density s as a function of coupling.

4.5.5. *Summary*

To summarize, I’ve tried to show you that, with enough work, it is possible to construct an effective Boltzmann equation that can be used for *leading*-order calculations of hydrodynamic transport. The methodology is far less systematic than for Euclidean field theories. In particular, going beyond leading order is challenging!

In looking at the real-time behavior, we also encountered a new scale, $g^4 T$, beyond the ones summarized earlier in Sec. 2.6:

- $g^2 T$: rate for small-angle scattering.
- $g^4 T$: rate for large-angle scattering.

A cartoon of the hierarchy of distance scales is shown in Fig. 23.

^sFor a textbook discussion, see Sec. 41 of Ref. 23.

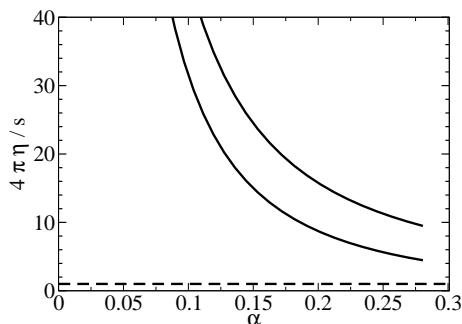


Fig. 22. Leading-order results adapted from Arnold, Moore and Yaffe⁴ for shear viscosity in 3-flavor QCD, as a function of α_s , in units of entropy density s over 4π . [The leading-order value of $s/4\pi$ is $\pi T^3(8/45 + 7N_f/60)$.] The two solid lines show two different calculations that should agree at leading order in coupling but differ at higher order, giving an idea of some of the possible errors from higher-order effects. The dashed line shows a conjectured lower bound on $\eta/4\pi s$ for any relativistic system.²⁴

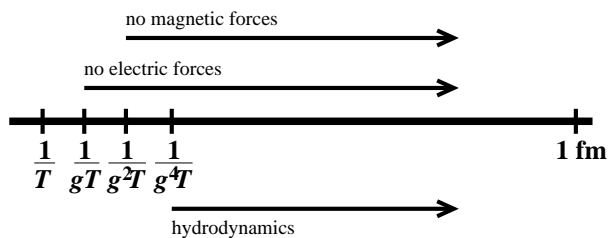


Fig. 23. A cartoon of distance scales relevant to high-temperature gauge theory.

5. Hard Loops and the Vlasov Equations

Looking at Fig. 23, note that, because of magnetic confinement, the long distance effective theory of a quark-gluon plasma is hydrodynamics and not the *magneto*-hydrodynamics (MHD) relevant to traditional electromagnetic plasmas. So, in some ways, non-abelian plasmas are a lot simpler than traditional electromagnetic plasmas, because there are no magnetic forces over large distances, like those responsible for the complicated structure of solar filaments.

Does that mean that there are no interesting collective effects in quark-gluon plasmas analogous to the rich variety of phenomena in traditional plasma physics? Not quite. There is a window of distance scales l ,

$$\frac{1}{T} \ll l \ll \frac{1}{g^2 T}, \quad (79)$$

large compared to the inter-particle separation but small compared to the magnetic screening length, which is large enough for collective effects yet small enough for magnetic and sometimes electric effects. An example we've already seen are low-momentum longitudinal plasma waves, whose collective nature was depicted in Fig.

8, where the characteristic scale was the plasma frequency $\omega_{\text{pl}} \sim gT$.

Our earlier discussion of plasma waves arose by considering one loop self-energies like Fig. 6, which were dominated by hard loop momenta $p \sim T$ and which had a significant effect on the propagation of low-momentum plasma waves. Such a loop is called a “hard thermal loop.” For imaginary-time physics, the self-energy turns out to be the end of the story as far as hard thermal loops are concerned. For real-time physics, however, Braaten and Pisarski²⁵ discovered some years ago that other one-loop diagrams such as Fig. 24 give important hard thermal loops, creating significant interactions between low momentum (e.g. $k \sim gT$) gluons. They found that all such interactions could be described by an effective Lagrangian for low-momentum gluons:

$$\mathcal{L}_{\text{eff}} = -\frac{m_{\text{D}}^2}{2} \left\langle F_{\mu\nu}^a \frac{v^\mu v^\rho}{(v \cdot D)^2} F_\rho^{b\nu} \right\rangle_{\mathbf{v}}, \quad (80)$$

where $v^\mu \equiv (1, \mathbf{v})$ with \mathbf{v} a unit vector,[†] and the angle brackets denote averaging over the direction of \mathbf{v} . This looks complicated and non-local because there is a covariant derivative D in the *denominator*. However, it turns out that there is simple, local physics that underlies this result, to which I now turn.

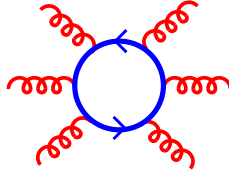


Fig. 24. A generic hard thermal loop. The internal line has $p \sim T$ and the external lines are soft ($k \ll T$).

5.1. The Vlasov Equations

For simplicity, let’s start with a QED plasma. Like in the picture of Fig. 8 of a longitudinal plasma wave, we want a description of (i) long wavelength (e.g. $\lambda \sim 1/gT$) fluctuations in the densities of hard ($p \sim T$) particles, coupled to (ii) soft ($k \sim gT$) gauge fields. Also, at these scales, we can ignore random, incoherent, two-particle collisions, because we are interested in physics in the window (79), which is restricted to distances small compared to the mean free path $\tau_{2 \rightarrow 2} \sim 1/g^2 T$ of such collisions.

Let’s start by re-examining the Boltzmann equation. Since we can ignore collisions in this context, we start with

$$\frac{df}{dt} = C = 0. \quad (81)$$

[†]Note: The notation v^μ is convenient, but v^μ does not transform as a 4-vector.

By the chain rule,

$$\frac{\partial f}{\partial t} + \frac{\partial \mathbf{x}}{\partial t} \cdot \frac{\partial f}{\partial \mathbf{x}} + \frac{\partial \mathbf{p}}{\partial t} \cdot \frac{\partial f}{\partial \mathbf{p}} = 0, \quad (82)$$

where (unlike earlier discussion) I allow for a common force $\mathbf{F} = \partial \mathbf{p} / \partial t$ on the particles due to the influence of the soft gauge fields that we want to incorporate.^u Substituting in the usual form of the electromagnetic force,

$$[\partial_t + \mathbf{v} \cdot \nabla_{\mathbf{x}} + g(\mathbf{E} + \mathbf{v} \times \mathbf{B}) \cdot \nabla_{\mathbf{p}}] f = 0. \quad (83a)$$

We combine this with Maxwell's equations for the soft field, with current given by the hard particles:

$$\partial_\mu F^{\mu\nu} = j^\nu = g \int_{\mathbf{p}} v^\nu f. \quad (83b)$$

(I have suppressed here an implicit sum over particle types.) The two equations (83) are known as the Vlasov equations.

To investigate thermal systems, linearize the distribution of particles in small fluctuations δf around thermal equilibrium f_{eq} ,

$$f(\mathbf{x}, \mathbf{p}, t) = f_{\text{eq}}(\mathbf{p}) + \delta f(\mathbf{x}, \mathbf{p}, t), \quad (84)$$

to get

$$(\partial_t + \mathbf{v} \cdot \nabla_{\mathbf{x}}) \delta f = -g(\mathbf{E} + \mathbf{v} \times \mathbf{B}) \cdot \nabla_{\mathbf{p}} f_{\text{eq}}, \quad (85a)$$

$$\partial_\mu F^{\mu\nu} = g \int_{\mathbf{p}} v^\nu \delta f. \quad (85b)$$

For QCD, the net color of the hard particles is treated quantum mechanically,^v $f(\mathbf{x}, \mathbf{p}, t)$ becomes a color density matrix, and space-time derivatives become covariant derivatives. In the linearized version (85), f_{eq} is color neutral, and δf can be taken in the adjoint representation, giving^w

$$(D_t + \mathbf{v} \cdot \mathbf{D}_{\mathbf{x}}) \delta f = -g(\mathbf{E} + \mathbf{v} \times \mathbf{B}) \cdot \nabla_{\mathbf{p}} f_{\text{eq}}, \quad (86a)$$

$$D_\mu F^{\mu\nu} = g \int_{\mathbf{p}} v^\nu \delta f. \quad (86b)$$

(I have suppressed here some numerical group factors.) These are local equations. but if we formally solve (86a) for δf and plug into (86b), we get a non-local equation for the evolution of the soft fields A :^x

$$D_\mu F^{\mu\nu} = -g^2 \int_{\mathbf{p}} v^\nu (D_t + \mathbf{v} \cdot \mathbf{D})^{-1} (\mathbf{E} + \mathbf{v} \times \mathbf{B}) \cdot \nabla_{\mathbf{p}} f_{\text{eq}}. \quad (87)$$

^uThese fields weren't relevant in our previous discussion of hydrodynamics because of magnetic confinement on the relevant distance scales.

^vThere are some versions that approximate the color as classical.

^wSee Ref. 26 for early work on kinetic theory and Ref. 27 for its application to HTL's.

^xI should mention that the $\mathbf{v} \times \mathbf{B} \cdot \nabla_{\mathbf{p}} f_{\text{eq}}$ term in (86a) and (87) vanishes, because an equilibrium distribution $f_{\text{eq}}(\mathbf{p})$ (Bose or Fermi) cares only about $|\mathbf{p}|$, so $\nabla_{\mathbf{p}} f_{\text{eq}}$ is in the direction of $\hat{\mathbf{p}} = \hat{\mathbf{v}}$ and so vanishes when dotted into $\mathbf{v} \times \mathbf{B}$. I have kept the term because in non-equilibrium applications (such as for the plasma instabilities discussed later), one wants to expand around non-isotropic distributions $f_0(\mathbf{p})$ rather than $f_{\text{eq}}(\mathbf{p})$, and in that case the $\mathbf{v} \times \mathbf{B}$ terms will not vanish.

This turns out to be equivalent to the equation of motion that you get from the HTL Lagrangian (80). The moral is that the physics is local, described by (86), provided you write it in terms of the full set of long-distance degrees of freedom in the theory: the soft fields A and the long-wavelength fluctuations δf in particle distributions.

5.2. *The self-energy revisited*

As an example, I'll outline how to use the Vlasov equation to derive the soft gluon self-energy. To do so, it's sufficient to treat the gluons perturbatively, so that the soft field A is a small quantity like δf . Then the linearized QCD Vlasov equations (86) reduce in form to the QED case (85). Fourier transform the Boltzmann equation (85a) ,

$$i(-\omega + \mathbf{v} \cdot \mathbf{k})\delta f = -g(\mathbf{E} + \mathbf{v} \times \mathbf{B}) \cdot \nabla_{\mathbf{p}} f_{\text{eq}}, \quad (88)$$

solve for δf , and plug into the Maxwell equation,

$$\partial_{\mu} F^{\mu\nu} = g \int_{\mathbf{p}} v^{\nu} \delta f = -ig^2 \int_{\mathbf{p}} \frac{v^{\nu}(\mathbf{E} + \mathbf{v} \times \mathbf{B})}{-\omega + \mathbf{v} \cdot \mathbf{k}} \cdot \nabla_{\mathbf{p}} f_{\text{eq}}. \quad (89)$$

Write this as $\partial_{\mu} F^{\mu\nu} = \Pi^{\nu\rho} A_{\rho}$ and extract Π . If you do this, you get the standard result for the soft gluon self-energy $\Pi(\omega, \mathbf{k})$ that you would get if you instead did the one-loop diagrammatic calculation discussed in Sec. 2.4. Kinetic theory (here in the form of the Vlasov equations) reproduces the same result one obtains from thermal loop calculations in the underlying quantum field theory.

6. Far from Equilibrium: Plasma Instabilities

I now want to investigate thermalization in cases that start far from equilibrium. To motivate the sort of question I want to ask, I'm going to start with a cartoonish description of a heavy ion collision.

6.1. *QGP hydrodynamics and elliptic flow*

The left-hand side of Fig. 25 shows a picture of a heavy ion collision, looking down the beam pipe. The nuclei are two Lorentz-contracted pancakes, represented by the large circles. One nucleus is heading towards you, out of the page, and the other nucleus is heading into the page. In general, they won't collide perfectly head on, and so there will be an almond shaped collision region, as shown. What if nothing interesting happened in heavy ion collisions? What if the result just looked like a bunch of independent nucleon-nucleon collisions, the products of which flew freely straight out to the detector? The debris of each nucleon-nucleon collision would (statistically) be isotropic in the transverse plane of the paper. So, if I looked at the transverse momentum distribution of particles seen in the detector, it would look rotationally invariant around the beam axis for each heavy ion collision, as depicted by the right-hand side of Fig. 25.

Now suppose that the products of the nucleon-nucleon collisions can't fly freely out, because they collide with the products of other nucleon-nucleon collisions on the way. And suppose that there are enough collisions that these particles, at least briefly, come to approximate local thermal equilibrium (e.g. a locally thermalized quark-gluon plasma). Imagine a time slightly after the collision, where the two nuclear pancakes have passed beyond each other, but the almond region is filled up into an almond cross-sectioned cylinder between the two. Outside that "cylinder" is vacuum, with zero pressure. In the center is some central pressure, and there will be a smooth gradient between the two, depicted by the contour lines in the upper left-hand figure in Fig. 26. As you can see from the figure, the pressure gradient must be larger along the short diameter of the almond. Pressure gradients correspond to forces, and so fluid elements along the short diameter will get accelerated (to the right and left) more than elements along the long diameter (accelerated up and down in the diagram). As a result of this anisotropic acceleration, the final products of the collision, when they finally split up and fly out to the detector, will (in a single heavy-ion collision) have an anisotropic distribution in lab-frame *transverse* momentum, as shown by the upper right-hand figure in Fig. 26. The acceleration of fluid elements is an example of hydrodynamic flow, and this particular manifestation is called "elliptic flow."

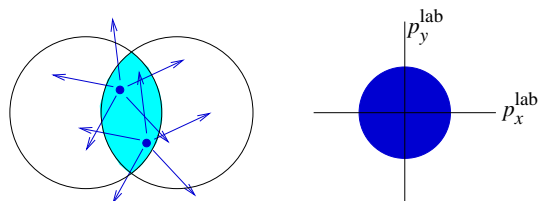


Fig. 25. A heavy ion collision if it were a superposition of independent nucleon-nucleon collisions.

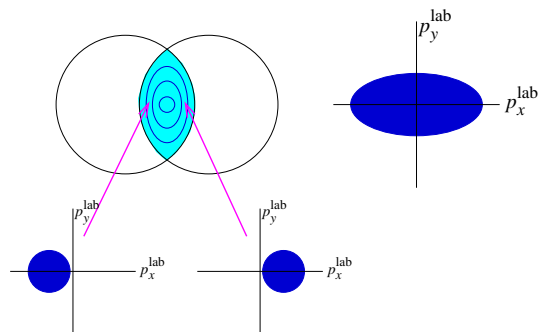


Fig. 26. Elliptic flow in a heavy ion collision.

In order to keep things straight in the discussion that follows, it will be important to distinguish between momentum of (i) all the particles in the lab frame, and (ii) local sets of particles in a local fluid frame. In the second case, I mean momenta as measured by an observer moving with the fluid (plasma), who only looks at particles that are close to her. In the hydrodynamic picture, elliptic flow is caused by pressure, which arises because of local thermalization. But in a thermal medium, momentum distributions are *isotropic* in local fluid rest frames. The lower part of Fig. 26 depicts two such isotropic distributions, one for a fluid element moving to the left and one to the right, boosted to the lab frame. Though each distribution is isotropic in its local fluid frame, their superposition is anisotropic in the lab frame. So, isotropization of momentum (via collisions) in local fluid rest frames creates pressure and ultimately produces anisotropic momenta (the signal of elliptic flow) in the *lab* frame.

The sooner collisions develop pressure, the sooner hydrodynamic flow can kick in, and the more significant will be elliptic flow. (If it takes too long, then the almond will in the meantime expand by free streaming into something bigger and more nearly circular, and so the difference between the two transverse directions will be less significant.) Matching simulations of ideal hydrodynamics to experimental data has led to a number of successes,^y but only if the system thermalizes very rapidly, on a time scale less than 1 fm/c. An important phenomenological question is whether such fast thermalization is reasonable. Can a quark-gluon plasma reach local thermal equilibrium in that short a time?

So here’s a question for theorists: What is the thermalization time for a quark-gluon plasma? That sounds hard, so let’s start with baby steps by asking a simpler question: What is it in the limit of arbitrarily weak coupling? As I mentioned in the introduction, even this problem is hard enough that we don’t even know how the answer scales with coupling!

$$t_{\text{eq}} \sim \frac{g^{-??}}{\text{momentum scale}}. \quad (90)$$

I’ll now explain what the difficulty is.

6.2. *Bottom-up thermalization*

In a wonderful 2000 paper, Baier, Mueller, Schiff and Son¹⁹ analyzed the effect of individual particle collisions on thermalization and determined the power “??” in (90) to be 13/5. There’s something they missed in their analysis, which is the difficulty I will get to shortly. But first, let me give an idea of the process of thermalization they found, which they called “bottom-up” thermalization.

Imagine that the heavy-ion collision takes place at position $z = 0$ along the beam axis. This is the point where I make contact with Francois Gelis’s talk.¹ At high energies, it’s expected that a very large (non-perturbatively large) density of (low x)

^ySee, for example, Ref. 28.

gluons are scattered out of the beam, and that these gluons are what's left behind from the collision to eventually form the quark-gluon plasma. (This initial state is called the color glass condensate and is described at early times using classical field theory, but we won't need to concern ourselves with those details here.) In what follows, I will refer to these initial scattered gluons as “hard” particles (even though they are quite low momentum compared to the initial nucleons that produced them) because I will reserve the term “soft” for yet lower momentum scales.

As the system expands in the space between the retreating, fragmented nuclei, it dilutes, and eventually the gluon density is no longer non-perturbative, and we can think of the system as a gas of individual gluons. As a first, crude approximation, let's ignore interactions and think of the gluons as free streaming. The only gluons that will hang around in the neighborhood $z = 0$ of the initial collision will be those with a small z component v_z of velocity: the gluons with significant v_z move to a different z . So, after a while, the momentum distribution of those gluons in the neighborhood of $z = 0$ starts to look very anisotropic, as shown in Fig. 27.^z In fact, the system looks similar (up to a boost) at other values of z . The only particles to get to the neighborhood of z at time t will be those with $v_z \simeq z/t$. If I boost by this amount to go to the “local fluid rest frame,” I'll again get the situation of Fig. 27.

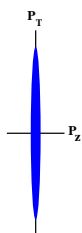


Fig. 27. An anisotropic local momentum distribution created by p_z selection as the system expands in the beam direction after the collision.

The process of bottom-up thermalization is shown in Fig. 28. Diagram (a) depicts a momentum distribution similar to Fig. 27. However, the particles are not free streaming: they interact via small angle collisions such as shown below diagram (a). Such collisions broaden p_z slightly, competing against the effect of expansion to shrink the local p_z distribution. So diagram (a) is broader in p_z than Fig. 27. Secondly, such collisions are occasionally accompanied by bremsstrahlung gluons, of which soft gluons are the most common. The circular area inside the momentum distribution of diagram (a) depicts these bremsstrahlung gluons. It's easier

^zNote that this is anisotropy in a local rest frame (and also is isotropic in the transverse plane) and has nothing to do with the anisotropy of elliptic flow. Quite the opposite: this local anisotropy represents, so far, a *failure* to thermalize.

to deflect a lower momentum particle than a higher momentum particle, so these softer gluons can fairly easily thermalize via collisions. (It's called bottom-up thermalization because the lowest momentum particles thermalize first.) Eventually, enough of these soft, bremsstrahlung gluons get produced, as indicated in diagram (b), that the hard particles favor scattering off of them rather than other hard particles. And eventually, there are so many soft particles to scatter from, that the relatively rare process of significant energy loss during bremsstrahlung becomes important. At that point, the energy stored in the hard particles rapidly cascades to lower momentum particles, as depicted below diagram (b), leaving us with the final thermalized plasma in diagram (c).

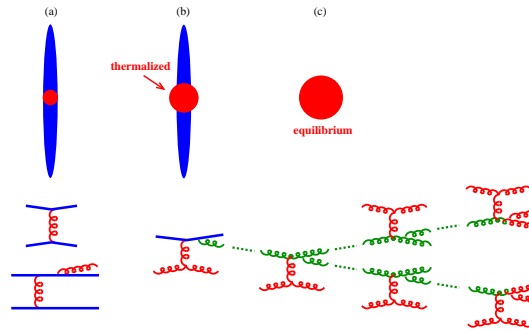


Fig. 28. Bottom-up thermalization.

So what's the problem? The problem is that plasma physics is complicated. There can be collective effects that are not captured by the independent, random particle collisions considered in the original bottom-up scenario. And one class of such effects is plasma instabilities.

6.3. *The Weibel (filamentation) instability*

The instability I will describe arises in non-equilibrium situations where particle momenta are anisotropic in local fluid frames. As an extreme example, think of ordinary electromagnetism and consider Fig. 29a, which depicts two homogeneous inter-penetrating currents of charged particles: one set of particles heading up the page, and the other down. Now, just to simplify my explanation, pretend that these particles were running through wires. Each line in Fig. 29a represent two wires on top of each other, one with a current up the page and one with a current down. Now recall from freshman physics (or use your right hand) that parallel currents attract and opposite currents repel. So the wires are unstable to clumping, as shown in Fig. 29b. The up-going wires want to get near each other and away from the down-going wires; the down-going wires want the same. Associated with these filaments are magnetic fields (which are causing the attraction and repulsion

of the wires), shown coming in and out of the paper by the crosses and circles in Fig. 29c. This instability is called the Weibel or filamentation instability and was discovered theoretically in 1959.²⁹

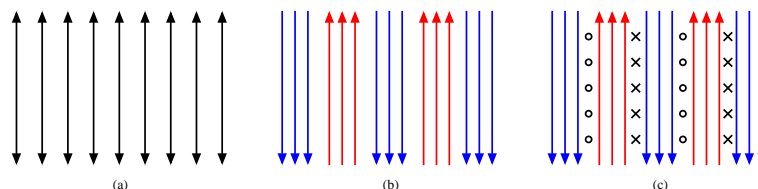


Fig. 29. The Weibel instability

The instability growth rate turns out to be much faster than the rate of individual particle collisions, and instabilities create relatively large soft magnetic fields. The hard particles of the bottom-up scenario depicted in Fig. 28 can scatter from these fields rather than from each other or soft particles created by bremsstrahlung. Unfortunately, all the details have not yet been worked out.

I would love to tell you more about Weibel instabilities,³⁰ and how their fate in QCD plasmas differs from traditional electromagnetic plasmas,³¹ and why this is important for understanding thermalization.³² I'd like to be able to tell you how the development of instabilities can be simulated by simulating the QCD Vlasov equations (86).^{31,33} And I'd like to explain what's left that needs to be done to complete the picture of thermalization at weak coupling. Unfortunately, I have run out of the pages allocated to writing up these lectures.

Acknowledgements

I thank the organizers of X Hadron Physics for inviting me to give these lectures. I am also indebted to my long-time collaborators, Guy Moore and Larry Yaffe. This work was supported, in part, by the U.S. Department of Energy under Grant No. DE-FG02-97ER41027.

References

1. See these proceedings and F. Gelis, T. Lappi and R. Venugopalan, arXiv:0708.0047 [hep-ph].
2. K. Kajantie, M. Laine, K. Rummukainen and Y. Schroder, *Phys. Rev.* **D67** (2003) 105008.
3. P. Arnold and L. G. Yaffe, *Phys. Rev.* **D52** (1995) 7208.
4. P. Arnold, G. D. Moore and L. G. Yaffe, *JHEP* **05** (2003) 051.
5. D. Bodeker, *Phys. Lett.* **B426** (1998) 351; P. Arnold, D. T. Son and L. G. Yaffe, *Phys. Rev.* **D59**, (1999) 105020.
6. F. Karsch and E. Laermann, arXiv:hep-lat/0305025.
7. S. S. Gubser, I. R. Klebanov and A. W. Peet, *Phys. Rev.* **D54** (1996) 3915.

8. E. Shuryak, *Prog. Part. Nucl. Phys.* **53** (2004) 273; M. Gyulassy and L. McLerran, *Nucl. Phys.* **A750** (2005) 30.
9. J. P. Blaizot, E. Iancu and A. Rebhan, *Phys. Rev.* **D68** (2003) 025011.
10. J. I. Kapusta and C. Gale, *Finite-Temperature Field Theory: Principles and Applications*, 2nd edition (Cambridge Univ. Press, 2006); M. Le Bellac, *Thermal Field Theory* (Cambridge Univ. Press, 1996).
11. D. A. Kirzhnits and A. D. Linde, *Annals Phys.* **101** (1976) 195; S. Weinberg, *Phys. Rev.* **D9** (1974) 3357; L. Dolan and R. Jackiw, *Phys. Rev.* **D9** (1974) 3320.
12. A. Gynther, M. Laine, Y. Schroder, C. Torrero and A. Vuorinen, *JHEP* **04** (2007) 094.
13. O. K. Kalashnikov and V. V. Klimov, *Yad. Fiz.* **31** (1980) 1357 [*Sov. J. Nucl. Phys.* **31** (1980) 699]; H. A. Weldon, *Phys. Rev.* **D26** (1982) 1394.
14. J. D. Jackson, *Classical Electrodynamics*, 2nd edition (John Wiley & Sons, 1975).
15. R. P. Feynman, R. B. Leighton, and M. Sands, *The Feynman Lectures on Physics*, vol. II (Addison-Wesley, 1977).
16. S. Weinberg, *Gravitation and Cosmology* (John Wiley & Sons, 1972).
17. S. Jeon, *Phys. Rev.* **D52** (1995) 3591; S. Jeon and L. G. Yaffe, *Phys. Rev.* **D53** (1996) 5799.
18. S. Klein, *Rev. Mod. Phys.* **71** (1999) 1501.
19. R. Baier, A. H. Mueller, D. Schiff and D. T. Son, *Phys. Lett.* **B502** (2001) 51.
20. P. Arnold, G. D. Moore and L. G. Yaffe, *JHEP* **01** (2003) 030.
21. P. Arnold, G. D. Moore and L. G. Yaffe, *JHEP* **0206** (2002) 030.
22. R. Baier, Y. L. Dokshitzer, A. H. Mueller, S. Peigne and D. Schiff, *Nucl. Phys.* **B483** (1997) 291; *ibid.* **B484** (1997) 265; B. G. Zakharov, *JETP Lett.* **63** (1996) 952; *ibid.* **65** (1997) 615; *Phys. Atom. Nucl.* **61** 838 (1998) [*Yad. Fiz.* **61** (1998) 924]; M. Gyulassy and X. N. Wang, *Nucl. Phys.* **B420** (1994) 583;
23. E. M. Lifshitz and L. P. Pitaevski, *Physical Kinetics* (Butterworth-Heinemann, 1995).
24. P. Kovtun, D. T. Son and A. O. Starinets, *Phys. Rev. Lett.* **94**, 111601 (2005).
25. E. Braaten and R. D. Pisarski, *Nucl. Phys.* **B337** (1990) 569.
26. U. Heinz, *Annals Phys.* **161** (1985) 48; *ibid.* **168** (1986) 148;
27. P. F. Kelly, Q. Liu, C. Lucchesi and C. Manuel, *Phys. Rev.* **D50** (1994) 4209.
28. U. W. Heinz, *AIP Conf. Proc.* **739** (2005) 163 [arXiv:nucl-th/0407067]; P. Huovinen and P. V. Ruuskanen, *Ann. Rev. Nucl. Part. Sci.* **56** (2006) 163.
29. E. S. Weibel, *Phys. Rev. Lett.* **2** (1959) 83.
30. S. Mrowczynski, *PoS C* **POD2006** (2006) 042 [arXiv:hep-ph/0611067]; P. Arnold, J. Lenaghan and G. D. Moore, *JHEP* **0308** (2003) 002.
31. P. Arnold, G. D. Moore and L. G. Yaffe, *Phys. Rev.* **D72** (2005) 054003; A. Rebhan, P. Romatschke and M. Strickland, *JHEP* **0509** (2005) 041; P. Arnold and G. D. Moore, *Phys. Rev.* **D73** (2006) 025006.
32. D. Bodeker, *JHEP* **0510** (2005) 092; P. Arnold and G. D. Moore, arXiv:0706.0490 [hep-ph].
33. D. Bodeker and K. Rummukainen, arXiv:0705.0180 [hep-ph].